IEEE Access
Multidisciplinary | Rapid Review | Open Access Journal

Received December 30, 2019, accepted January 3, 2020, date of publication January 8, 2020, date of current version January 17, 2020.

Digital Object Identifier 10.1109/ACCESS.2020.2964947

Active Fault Tolerant Control of Adaptive Cruise Control System Considering Vehicle-Borne Millimeter Wave Radar Sensor Failure

HUA ZHANG, (Fellow, IEEE), JUN LIANG, AND ZHIYUAN ZHANG
State Key Laboratory of Industrial Control Technology, Zhejiang University, Hangzhou 310000, China

Corresponding author: Jun Liang (jliang@zju.edu.cn)

This work was supported in part by the National Natural Science Foundation of China under Grant U1664264, and in part by the National Key Research and Development Program of China under Grant 2019YFB1600500.

ABSTRACT Vehicle-borne millimeter wave radar sensor may malfunction during signal acquisition and transmission process, which will affect the decision of adaptive cruise control (ACC) system and the safe driving of vehicles. However, adding other redundant environment-aware devices will increases costs. Therefore, in this paper, an active fault tolerant control of ACC system considering vehicle-borne millimeter wave radar sensor failure is proposed. Sensor faults are taken as discrete events, and the mixed logical dynamical (MLD) model of ACC upper control system is built which includes both the fault-free dynamics and the fault dynamics of the system. Then, the active fault tolerant control model of ACC system is established based on model predictive control (MPC) framework. Compared with the existing researches, this work emphasizes on the active fault tolerant control without adding other redundant environment-aware devices, which has not been fully revealed by the existing researches and is important to the industrial application. Moreover, the active fault tolerant control method can be easily ported to other driver assistance system besides ACC. The simulation results show that the vehicle equipped with the active fault tolerant ACC system can still drive safely and smoothly without being affected by radar sensor failures, which demonstrates its great significance to improve vehicle's own intelligence and ensure the safe driving instead of relying entirely on sensors.

INDEX TERMS Active fault tolerant, adaptive cruise control, intelligent vehicles, mixed logical dynamical model, model predictive control.

I. INTRODUCTION

As the key to ensuring the highway traffic security, adaptive cruise control (ACC), lane departure warning (LDW) and other advanced driver assistance system (ADAS) technologies have increasingly attracted people's attention [1]–[3]. ACC, also known as the active cruise control system, combining the cruise control at constant speed and the control of vehicle distance keeping, adopting vehicle-borne radar for environmental perception, thus assists the driver to drive the car safely and comfortably [4]–[6]. At present, the ACC system is configured on some brands' high-end cars, and its functions are also expanding.

As an important part of ACC for environmental perception, vehicle-borne millimeter wave radar can detect obstacle targets within a certain range around the ego vehicle in real time [7]. However, in the acquisition and transmission process of millimeter wave radar signals, due to the interference of the external environment or the failure of radar devices, the measured value of the dynamics state of the target vehicle will inevitably contain certain measurement noises, and the fault conditions such as missing detection and false detection may occur [8]. In this case, the accuracy of vehicle-borne millimeter wave radar is relatively low and does not satisfy the requirements of vehicle active safety control system [9]. Even a very short failure may cause a driving accident. One solution is to use multi-sensor fusion, such as configuring lidar, but requires a lot of cost. Another solution is to get information about the surrounding vehicles through V2V communication, but this technology is not yet popular and wireless communication network may temporarily fail [10]. Therefore, without the addition of other redundant environment-aware devices,

The associate editor coordinating the review of this manuscript and approving it for publication was Bohui Wang.

researching the active fault tolerant control of ACC system in the condition of vehicle-borne millimeter wave radar sensor faults is of great significance. This research can improve vehicle's own intelligence to ensure the safe driving instead of relying entirely on sensors.

At present, there is not much research in this problem. Guo and Yue [11] established a switched sampled-data cooperative adaptive cruise control (CACC) system model considering the effect of the onboard infrared sensor failure, and then designed state feedback controllers to stabilize the CACC system. They supposed that all following vehicles have the same sensor failure and they divided sensor failure into complete failure and partial failure, which values are all smaller than the true value. However, that is almost impossible in practice because the fault value of each sensor are random. Nunen *et al.* [12] present an algorithm of a Safety Checker which determines in real time the safe headway time and safe standstill distance for an ACC system, but they took the inaccuracies of radar failure as white noise and ignored effects of missing detection and false detection. Boukhari [13] presented two fault tolerant schemes to handle the autonomous vehicle speed sensor's additive faults, but they didn't consider sensor faults of vehicle-borne radar which has serious impact on environmental perception.

The ACC system, enabling ACC-equipped vehicles to drive safely on the condition of noise interference and failure of vehicle-borne millimeter wave radar sensor. Based on this purpose, in this paper, sensor faults are taken as discrete events, and the mixed logical dynamical (MLD) model of ACC upper control system is built which includes both the fault-free dynamics and the fault dynamics of the system. Based on model predictive control (MPC) framework and the MLD model, the active fault tolerant control model of ACC system is established. The main contributions of this study are as follows:

1) Our work lays emphasis on the active fault tolerant control on the condition of vehicle-borne millimeter wave radar sensor failure without adding other redundant environment-aware devices, which has not been revealed by the existing researches and is important to the industrial application.

2) Our work improves on the traditional MPC-based ACC system, and fuses the MLD model with the MPC framework. The method is simple and easy to understand, and achieves sound effects of active fault tolerance control.

3) Besides ACC, methods of vehicle dynamic state estimation, sensor fault recognition and the active fault tolerant control model proposed in this paper can be easily ported to other advanced driver assistance system technologies, such as collision avoidance system and lane change assist system.

Combined with the PreScan vehicle simulation platform, the application of the proposed active fault tolerant control algorithm of ACC system is tested in complex traffic scenarios.

The simulation results show that for the millimeter wave radar sensor failure in extreme cases, the active fault tolerant ACC system can accurately recognize the false detection and missing detection of the radar sensor, and then implement the active fault tolerant control to maintain the desired relative distance and smooth velocity response. This novel method is of great significance to ensure the safe driving of intelligent vehicles.

The structure of the paper is as follows. Section 2 presents vehicle dynamic state estimation and sensor fault recognition based on vehicle-borne millimeter wave radar signal. Section 3 builds the MLD model of ACC upper control system considering sensor faults. Section 4 presents an active fault tolerant control model of vehicle ACC system based on the MPC framework. Section 5 presents the results of simulation and analysis in complex traffic scenarios. Finally, section 6 draws the conclusion.

II. VEHICLE DYNAMIC STATE ESTIMATION AND SENSOR FAULT RECOGNITION BASED ON VEHICLE-BORNE MILLIMETER WAVE RADAR SIGNAL

In complex traffic scenarios, an ACC-equipped vehicle needs to rely on the vehicle-borne millimeter wave radar sensor to detect surrounding vehicles, and determine whether to enter a cruising mode or a following mode by detecting vehicles in the same lane in a certain range ahead. In a following mode, it is necessary to smoothly follow the change of the target vehicle while maintaining the safe relative distance. The target vehicle may change lane to leave, and the vehicles in adjacent lanes may also be inserted.

However, in the acquisition and transmission process of millimeter-wave radar signals, due to the interference of the external environment or the failure of radar devices, measured values of the target vehicle moving state will inevitably contain certain measurement noises, and fault conditions such as missing detection and false detection may occur. Measurement noises can be modeled as the white noise and reduced by filtering. While, the occurrence of sensor failures is random and unpredictable, which is difficult to describe with specific mathematical models. Missing detection means that the radar sensor signal is missing. False detection means that signals detected by the radar sensor has large errors. In this case, the accuracy of vehicle-borne millimeter wave radar is relatively low and does not satisfy the requirement of vehicle active safety control system. We cannot predict in advance when radar sensor faults will occur, nor can we predict in advance how much received signals deviate from actual values. Therefore, in the complex traffic environment, the millimeter wave radar data processing module applied to the ACC system needs to estimate actual vehicle dynamic states and recognize fault conditions of radar sensor when they occur.

A. VEHICLE DYNAMIC STATE ESTIMATION

In this paper, the Sage-Husa adaptive Kalman filtering algorithm is adopted to establish the vehicle dynamic state estimation model [10], [14]. It should be noted here that in order to avoid filter divergence problems and low estimation accuracy, we used Sage-Husa adaptive Kalman filtering algorithm

rather than the simpler classical Kalman filter or extended Kalman filter algorithm.

The vehicle-borne millimeter wave radar can detect the longitudinal relative distance ΔS_{x_radar}, longitudinal relative velocity Δv_{x_radar}, lateral relative distance ΔS_{y_radar} and lateral relative velocity Δv_{y_radar} of a certain target vehicle from the ego vehicle. Here, we take the longitudinal motion state estimation as an example, the lateral motion state of the target vehicle can also be estimated by the Sage-Husa adaptive Kalman filtering algorithm in the same way.

Here, it is assumed that the longitudinal relative jerk of the target vehicle from the ego vehicle is constant and is subject to zero-mean system random noise interference. Construct a continuous system state vector $X(t) = [\Delta S_x(t), \Delta v_x(t), \Delta a_x(t), \Delta j_x(t)]^T$, where $\Delta S_x(t)$, $\Delta v_x(t)$, $\Delta a_x(t)$, $\Delta j_x(t)$ are respectively the true longitudinal relative distance, true longitudinal relative velocity, true longitudinal relative acceleration, and true longitudinal relative jerk of this target vehicle from the ego vehicle at time t. According to the derivative differential relationship between the above physical quantities, the continuous state equation in the time domain of each physical quantity can be listed:

$$\dot{X}(t) = AX(t) + BW(t) \tag{1}$$

where A is the continuous system matrix, and $A = \begin{bmatrix} 0 & 1 & 0 & 0 \\ 0 & 0 & 1 & 0 \\ 0 & 0 & 0 & 1 \\ 0 & 0 & 0 & 0 \end{bmatrix}$. B is the continuous system noise driven matrix, and $B = [0, 0, 0, 1]^T$. $W(t)$ is the system noise, here is the zero-mean random relative jerk interference, which is a scalar.

The discrete similar method [15] in time domain is used to discretize the time domain continuous state equation in Eq. (1) at the time interval T that is the millimeter wave radar's measurement frequency, and a discrete system state space model is established:

system state equation:

$$X(k) = \Phi X(k-1) + \Gamma W(k-1) \tag{2}$$

observation equation:

$$Z(k) = HX(k) + V(k) \tag{3}$$

where $X(k) = \left[\Delta S_x(k), \Delta v_x(k), \Delta a_x(k), \Delta j_x(k)\right]^T$. $Z(k) = \left[\Delta S_{x\_radar}(k), \Delta v_{x\_radar}(k)\right]^T$ is the observation vector. $\Delta S_{x\_radar}(k)$, $\Delta v_{x\_radar}(k)$ are respectively the longitudinal relative distance, longitudinal relative velocity of this target vehicle from the ego vehicle detected by millimeter wave radar in the $\boldsymbol{k}$ th detection period. Φ is the one-step state transition matrix of the system from the $\boldsymbol{k-1}$ th detection period to the $\boldsymbol{k}$ th detection period, and $\Phi = e^{A \cdot T} = \sum_{k=0}^{\infty} \frac{A^k \cdot T^k}{k!} = \begin{bmatrix} 1 & T & \frac{T^2}{2} & \frac{T^3}{6} \\ 0 & 1 & T & \frac{T^2}{2} \\ 0 & 0 & 1 & T \\ 0 & 0 & 0 & 1 \end{bmatrix}$. Γ is the discrete system noise drive matrix, and $\Gamma = \int_0^T e^{A \cdot T} dt \cdot B = \sum_{k=1}^{\infty} \frac{A^{k-1} \cdot T^k}{k!} \cdot B = \left[\frac{T^4}{24}, \frac{T^3}{6}, \frac{T^2}{2}, T\right]^T$. $W(k-1)$ is the value of system random noise in the $\boldsymbol{k-1}$ th detection period. H is the observation matrix, and $H = \begin{bmatrix} 1 & 0 & 0 & 0 \\ 0 & 1 & 0 & 0 \end{bmatrix}$. $V(k)$ is the observation noise, and $V(k) = \begin{bmatrix} v_0(k) \\ v_1(k) \end{bmatrix}$. $v_0(k)$ is the error when measuring ΔS_x, and $v_1(k)$ is the error when measuring Δv_x.

The premise assumption of vehicle dynamic state estimation based on the Sage-Husa adaptive Kalman filtering algorithm is that the mean of system noise and observation noise is 0, the statistical properties of observation noise are approximately known and constant, and the statistical properties of system noise are unknown and time-varying. That is, the statistical properties of $W(k)$ and $V(k)$ in the state space model satisfy:

$$\begin{aligned} E[W(k)] &= 0, Cov[W(k), W(j)] \\ &= E\left[W(k) \cdot W(j)^T\right] = Q(k)\eta_{kj} \end{aligned} \tag{4}$$

$$\begin{aligned} E[V(k)] &= 0, Cov[V(k), V(j)] \\ &= E\left[V(k) \cdot V(j)^T\right] = R\delta_{kj} \approx \begin{bmatrix} R_0 & 0 \\ 0 & R_1 \end{bmatrix} \eta_{kj} \end{aligned} \tag{5}$$

$$Cov[W(k), V(j)] = E\left[W(k) \cdot V(j)^T\right] = 0 \tag{6}$$

where $\eta_{kj} = \begin{cases} 0, & k \neq j \\ 1, & k = j \end{cases}$. $Q(k)$ is the variance of the system random noise $W(k)$, and R is the variance of the observation noise $V(k)$. The approximate value of R can be obtained through a large number of experimental statistical analysis.

In order to solve filter divergence problems, the variable $S(k)$ is introduced to adjust filter gains indirectly. At the same time, when the statistical properties of system noise are estimated, if $\hat{Q}(k)$ loses positive semi-definite, the biased valuation of $\hat{Q}(k)$ is used instead of unbiased valuation to ensure positive semi-definite of $\hat{Q}(k)$. The steps of the Sage-Husa adaptive Kalman filter algorithm are as follows:

1)One-step state prediction:

$$\hat{X}(k|k-1) = \Phi \hat{X}(k-1|k-1) \tag{7}$$

2)Innovations equation:

$$\varepsilon(k) = Z(k) - H\hat{X}(k|k-1) \tag{8}$$

3) Filter divergence criterion:

$$\varepsilon(k)^T \varepsilon(k) \leq \xi \cdot T_r\left[HP(k|k-1)H^T + R\right] \tag{9}$$

where $\xi(\xi \geq 1)$ is a tunable coefficient. When $\xi = 1$, the above formula is the most stringent criterion. T_r is the trace of a matrix. If Eq. (9) holds, the filter does not diverge, but if Eq. (9) does not hold, the filter diverges.

4)Calculate the value of $S(k)$:

$$S(k) = \begin{cases} 1, & Eq.\ (9)\ holds \\ \dfrac{T_r\left[\varepsilon(k)\,\varepsilon(k)^T - H\Gamma\hat{Q}(k-1)\,\Gamma^T H^T - R\right]}{T_r\left[H\Phi P(k-1|k-1)\,\Phi^T H^T\right]}, & \\ & Eq.\ (9)\ does\ not\ hold \end{cases} \quad (10)$$

5) One-step prediction covariance matrix:

$$P(k|k-1) = \mathrm{S}(\mathrm{k})\,\Phi P(k-1|k-1)\,\Phi^T + \Gamma\hat{Q}(k-1)\,\Gamma^T \quad (11)$$

6) Filter gain:

$$K(k) = P(k|k-1)\,H^T\left[HP(k|k-1)\,H^T + R\right]^{-1} \quad (12)$$

7)State estimation:

$$\hat{X}(k|k) = \hat{X}(k|k-1) + K(k)\varepsilon(k) \quad (13)$$

8)Mean square error estimation:

$$P(k|k) = [I - K(k)\,H]P(k|k-1) \quad (14)$$

9)Subtractive memory index weighted sequence:

$$d(k-1) = \frac{1-b}{1-b^k} \quad (15)$$

where $d(k-1)$ is the subtractive memory index weighted sequence, which is used to reduce the effect of obsolete observation data in the process of real-time estimation of noise statistical properties and emphasize the effect of observation data at a nearer time. $b(0 < b < 1)$ is a forgetting factor, indicating the speed of forgetting old data items. The larger b is, the slower the forgetting speed is.

10) Statistical properties estimation of system noise:

If $\Gamma\hat{Q}(k)\,\Gamma^T$ is positive semi-definite,

$$\begin{aligned}\Gamma\hat{Q}(k)\,\Gamma^T &= [1-d(k-1)]\,\Gamma\hat{Q}(k-1)\,\Gamma^T + d(k-1) \\ &\times\left[K(k)\,\varepsilon(k)\,\varepsilon(k)^T K(k)^T + P(k|k) - \Phi P(k-1|k-1)\,\Phi^T\right]\end{aligned} \quad (16)$$

If $\Gamma\hat{Q}(k)\,\Gamma^T$ loses positive semi-definite,

$$\begin{aligned}\Gamma\hat{Q}(k)\,\Gamma^T &= [1-d(k-1)]\,\Gamma\hat{Q}(k-1)\,\Gamma^T \\ &+ d(k-1)\left[K(k)\,\varepsilon(k)\,\varepsilon(k)^T K(k)^T\right]\end{aligned} \quad (17)$$

Eq. (16) is an unbiased estimate of the system noise variance matrix. However, because of the matrix subtraction operation, it is easy to make $\Gamma\hat{Q}(k)\,\Gamma^T$ lose semi-positive definiteness or positive definiteness, which may lead to filter divergence problems. Therefore, if $\Gamma\hat{Q}(k)\,\Gamma^T$ loses semi-positive definiteness or positive definiteness, we use a biased estimate with only addition operation instead of the original unbiased estimate to ensure the positive definiteness of $\Gamma\hat{Q}(k)\,\Gamma^T$, as shown in Eq. (17).

In the simulation calculation below, the initial conditions of the filtering are explained.

Using the same method, the lateral motion state of the target vehicle can also be estimated by the Sage-Husa adaptive Kalman filtering algorithm.

FIGURE 1. Complex traffic scenario.

B. FAULT RECOGNITION OF VEHICLE-BORNE MILLIMETER WAVE RADAR SENSOR

The millimeter wave radar data processing module applied in an ACC system needs to identify the target vehicle in the same lane of ego vehicle and the vehicles in adjacent lanes on both sides of the ego vehicle among the numerous targets detected by millimeter-wave radar, and then recognize conditions of missing detection and false detection.

For the recognition of vehicles in the same lane and adjacent lanes, this paper adopts a simple method of lateral distance threshold, i.e.,

$$N_{same} = \left\{ i \middle| \left|\Delta\hat{S}_y^i(k)\right| \le Y_{same} \right\} \quad (18)$$

$$N_{adj} = \left\{ i \middle| Y_{same} < \left|\Delta\hat{S}_y^i(k)\right| \le Y_{adj} \right\} \quad (19)$$

where N_{same} is the set of same lane vehicles, N_{adj} is the set of adjacent lane vehicles, $\Delta\hat{S}_y^i(k)$ is the lateral relative distance of the ith vehicle from the ego vehicle in the $\boldsymbol{k}$ th detection period, $i = 1, 2, \ldots R_{max}$. R_{max} is the maximum number of objects that can be detected by vehicle-borne millimeter wave radar, Y_{same} is the threshold value of the same lane, Y_{adj} is the threshold value of adjacent lanes. A vehicle with the closest longitudinal relative distance from the ego vehicle in N_{same} is selected as the target vehicle. Vehicles with the closest longitudinal relative distance from the ego vehicle in N_{adj} are selected for state tracking.

For the fault recognition of vehicle-borne millimeter wave radar sensor in the $\boldsymbol{k}$ th detection period, this paper adopts the method shown in Fig.2.

According to Fig.2, firstly, the premise of sensor faults identification is to judge whether there are lane changing trends of the target vehicle and vehicles in the adjacent lanes.

Here, based on section II.A, dynamic state estimation models are built for lateral dynamic states of the target vehicle and vehicles in adjacent lanes, respectively. Then we can obtain predictive values of relative lateral distances and relative velocities of these vehicles from the ego vehicle in the $\boldsymbol{k+1}$ th detection period. According to the following method, lane changing trends can be judged.

$$If\ \left|\Delta\hat{S}_{y\_same}(k+1)\right| > Y_{same}\ \&\ \left|\Delta\hat{v}_{y\_same}(k+1)\right| \ne 0,\quad \lambda_{same}(k) = 1 \quad (20)$$

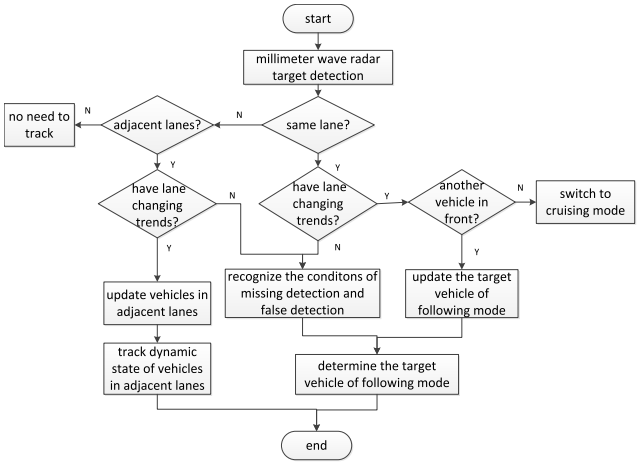

FIGURE 2. Fault recognition method of vehicle-borne millimeter wave radar sensor in the k th detection period.

$$If \ \left|\Delta\hat{S}^i_{y\_adj}(k+1)\right| \le Y_{same} \ \& \ \left|\Delta\hat{v}^i_{y\_adj}(k+1)\right| \ne 0, \quad \lambda^i_{adj}(k) = 1(i \in N_{adj}) \tag{21}$$

where $\Delta\hat{S}_{y\_same}(k+1)$ and $\Delta\hat{v}_{y\_same}(k+1)$ are predictive values of relative lateral distance and relative velocity between the target vehicle and the ego vehicle in the $\boldsymbol{k+1}$ th detection period, respectively. $\lambda_{same}(k)$ is the warning sign signal of the target vehicle in the $\boldsymbol{k}$ th detection period. If the target vehicle has the lane changing trend, $\lambda_{same}(k) = 1$, otherwise $\lambda_{same}(k) = 0$. $\Delta\hat{S}^i_{y\_adj}(k+1)$ and $\Delta\hat{v}^i_{y\_adj}(k+1)$ are predictive values of relative lateral distance and relative velocity between the ego vehicle and the i th vehicle in adjacent lanes in the $\boldsymbol{k+1}$ th detection period, respectively. $\lambda^i_{adj}(k)$ is the warning sign signal of this vehicle in the $\boldsymbol{k}$ th detection period.

Secondly, the fault recognition of radar sensor missing detection is carried out as follows.

$$If \ \lambda_{same}(k) = 0 \ \& \ Z_{same}(k) = [], \quad \delta 1_{same}(k) = 1 \tag{22}$$

$$If \ \lambda^i_{adj}(k) = 0 \ \& \ Z^i_{adj}(k) = [], \quad \delta 1^i_{adj}(k) = 1 \left(i \in N_{adj}\right) \tag{23}$$

where $Z_{same}(k)$ is the millimeter wave radar sensor observation of the target vehicle in the $\boldsymbol{k}$ th detection period, that is, $Z_{same}(k) = [\Delta S_{x\_same}, \Delta S_{y\_same}, \Delta v_{x\_same}, \Delta v_{y\_same}]^T$, and $Z_{adj}(k) = [\Delta S_{x\_adj}, \Delta S_{y\_adj}, \Delta v_{x\_adj}, \Delta v_{y\_adj}]^T$.

On the premise that the target vehicle does not change lane to leave, if $Z_{same}(k)$ is empty, it can be recognized as the condition of missing detection and the sign of missing detection $\delta 1_{same}(k) = 1$, otherwise $\delta 1_{same}(k) = 0$. $Z^i_{adj}(k)$ is the millimeter wave radar sensor observation of the ith vehicle in adjacent lanes in the $\boldsymbol{k}$ th detection period, and the same method can be used to identify missing detection conditions of this vehicle.

Finally, the fault recognition of radar sensor false detection is carried out as follows.

$$If \ \lambda_{same}(k) = 0 \ \& \ \lambda_{adj}(k) = 0 \ \& \ Z_{same}(k) \notin [Z_{same\_min}(k), Z_{same\_max}(k)], \quad \delta 2_{same}(k) = 1 \tag{24}$$

$$If \ \lambda_{same}(k) = 0 \ \& \ \lambda^i_{adj}(k) = 0 \ \& \ Z_{adj}(k) \notin [Z_{adj\_min}(k), Z_{adj\_max}(k)], \quad \delta 2^i_{adj}(k) = 1 \tag{25}$$

where in the $\boldsymbol{k}$ th detection period, on the premise that the target vehicle does not change the lane to leave and the vehicles in adjacent lanes do not change lanes to the front of the ego vehicle, if $Z_{same}(k)$ exceeds the threshold range $[Z_{same\_min}(k), Z_{same\_max}(k)]$, it can be recognized as the condition of false detection and the sign of false detection $\delta 2_{same}(k) = 1$, otherwise $\delta 2_{same}(k) = 0$.

$Z_{same}(k)$ can be written as:

$$Z_{same}(k) = \begin{bmatrix} \Delta S_{x\_same}(k) \\ \Delta S_{y\_same}(k) \\ \Delta v_{x\_same}(k) \\ \Delta v_{y\_same}(k) \end{bmatrix} = \begin{bmatrix} S_{x\_same}(k) - S_{x\_ego}(k) \\ \Delta S_{y\_same}(k) \\ v_{x\_same}(k) - v_{x\_ego}(k) \\ \Delta v_{y\_same}(k) \end{bmatrix} \tag{26}$$

where, S_{x_same} and S_{x_ego} are respectively the longitudinal distance of the target vehicle and the ego vehicle. v_{x_same} and v_{x_ego} are respectively the longitudinal velocity of the target vehicle and the ego vehicle.

It can be considered that during one detection period, the target vehicle is doing uniform acceleration motion. Then, $S_{x\_same}(k)$ and $v_{x\_same}(k)$ are described based on the kinematic distance and velocity formula:

$$S_{x\_same}(k) = v_{x\_same}(k-1) \cdot T + \frac{1}{2} a_{x\_same}(k-1) T^2 \tag{27}$$

$$v_{x\_same}(k) = v_{x\_same}(k-1) + a_{x\_same}(k-1) T \tag{28}$$

where, $v_{x\_same}(k-1)$ is the longitudinal velocity of the target vehicle in the $\boldsymbol{k-1}$ th detection period. a_{x_same} is the longitudinal acceleration of the target vehicle. According to references [16]–[18], in the normal braking process of ordinary vehicles (without considering super cars), the braking deceleration should generally not be greater than 0.4g, otherwise tires will be severely worn and passengers will feel uncomfortable. While, in the process of emergency braking, the maximum deceleration generally does not exceed 0.8g. Then, we set $a_{x\_min} \le a_{x\_same} \le a_{x\_max}$. Where, $a_{x\_min} = -8\text{m/s}^2$, and $a_{x\_max} = 4\text{m/s}^2$. Then, $Z_{same\_min}(k)$ and $Z_{same\_max}(k)$ can be calculated by:

$$Z_{same\_min}(k) = \begin{bmatrix} v_{x\_same}(k-1) \cdot T + \frac{1}{2} a_{x\_min} T^2 - S_{x\_ego}(k) \\ -Y_{same} \\ v_{x\_same}(k-1) + a_{x\_min} T - v_{x\_ego}(k) \\ -Y_{same}/T \end{bmatrix} \tag{29}$$

$$Z_{same\_max}(k) = \begin{bmatrix} v_{x\_same}(k-1) \cdot T + \frac{1}{2} a_{x\_max} T^2 - S_{x\_ego}(k) \\ Y_{same} \\ v_{x\_same}(k-1) + a_{x\_max} T - v_{x\_ego}(k) \\ Y_{same}/T \end{bmatrix} \tag{30}$$

From Eq. (29) and Eq. (30), it can be seen that the threshold setting is related to the velocity of the target vehicle in the $k-1$ th detection period, the set acceleration limit, the velocity and distance of the ego vehicle in the k th detection period. Such a threshold setting method can avoid mistaking potential abrupt braking event or lane departure of the target vehicle for radar sensor false detection.

Similarly, the condition of false detection of vehicles in adjacent lanes can be recognized.

Note here that if the condition of radar sensor failure is recognized, when estimating the vehicle dynamic state, it is necessary to eliminate the erroneous observation data to avoid the influence of the abnormal measurement data on the state estimation accuracy.

In this section, driving scenarios are defined, vehicle dynamic states are estimated adopting the Sage-Husa adaptive Kalman filtering algorithm, and fault conditions of vehicle-borne millimeter wave radar sensor are recognized using above methods. Signs of missing detection and false detection in each detection period are obtained, which will be used for MLD modeling of ACC upper control system in section 3.

III. MLD MODELING OF ACC UPPER CONTROL SYSTEM

A. VEHICLE-TO-VEHICLE LONGITUDINAL KINEMATICS MODEL

The longitudinal kinematics model of the ego vehicle and the vehicle in front of the same lane is built. The schematic diagram is shown in Fig.3. The vehicle in front of the same lane is the target vehicle mentioned above, and it is represented by subscript p in the following text.

It can be seen from Fig.3 that there are following longitudinal kinematics relationships between the ego vehicle and the front vehicle, as described in Eq. (31), Eq. (32), Eq. (33).

$$\Delta s\left(k\right) = s_p\left(k\right) - s_{ego}(k) \tag{31}$$

$$\Delta s_{des}\left(k\right) = d_0 + t_h \cdot v_{ego}(k) \tag{32}$$

$$\sigma\left(k\right) = \Delta s\left(k\right) - \Delta s_{des}\left(k\right) \tag{33}$$

where s_p is the longitudinal distance of the target vehicle; s_{ego} is the longitudinal distance of the ego vehicle; Δs is the actual longitudinal relative distance of these two vehicles; Δs_{des} is the desired longitudinal relative distance of these two vehicles; d_0 is a fixed longitudinal distance between two vehicles; t_h is the expected time headway; v_{ego} is the longitudinal velocity of the ego vehicle; σ is the error between Δs and Δs_{des}.

The value of the fixed longitudinal distance d_0 between two vehicles depends on the braking process and the vehicle following process. In the braking process, d_0 is the product of time-to-collision (TTC) and the velocity of the ego vehicle. In the vehicle following process, d_0 is the minimum safe distance d_c between two vehicles, which usually includes a vehicle length and a fixed distance value [3] as described in Eq. (34).

$$d_0 = \max\left\{t_{TTC} \cdot v_{ego}\left(k\right), d_c\right\} \tag{34}$$

The expected time headway t_h is related to factors such as the longitudinal velocity of the ego vehicle, the longitudinal velocity and acceleration of the target vehicle. If the fixed t_h is used, the influence of different driving conditions on time headway will be ignored [19], [20]. Therefore, variable t_h is adopted as described in Eq. (35).

$$t_h = b_1 - b_2 * v_{rel} - b_3 * a_p \tag{35}$$

where a_p is the longitudinal acceleration of the target vehicle, which is considered as the disturbance of the ACC system and is denoted as w in the following text; v_{rel} is the longitudinal relative velocity of the target vehicle and the ego vehicle; b_1, b_2, b_3 are parameters greater than 0.

According to the reference [21], the actual longitudinal acceleration a_{ego} and the desired longitudinal acceleration a_{des} of the ego vehicle satisfy the Eq. (36).

$$a_{ego}\left(k+1\right) = \left(1 - \frac{T_s}{\tau}\right) a_{ego}\left(k\right) + \frac{T_s}{\tau} a_{des}\left(k\right) \tag{36}$$

where T_s is the sampling period of the ACC system; τ is the time constant of ACC lower control; the desired longitudinal acceleration a_{des} is denoted as u in the following text which is the control input of ACC upper control model.

Following equations can be obtained from mutual longitudinal kinematics characteristics between the ego vehicle and the target vehicle:

$$\Delta s\left(k+1\right) = \Delta s\left(k\right) + v_{rel}\left(k\right) T_s + \frac{1}{2} w(k) T_s^2 - \frac{1}{2} a_{ego}(k) T_s^2 \tag{37}$$

$$v_{rel}\left(k+1\right) = v_{rel}\left(k\right) + w\left(k\right) T_s - a_{ego}(k) T_s \tag{38}$$

$$v_{ego}\left(k+1\right) = v_{ego}\left(k\right) + a_{ego}(k) T_s \tag{39}$$

$$a_{ego}\left(k+1\right) = \left(1 - \frac{T_s}{\tau}\right) a_{ego}\left(k\right) + \frac{T_s}{\tau} u(k) \tag{40}$$

$$j_{ego}\left(k+1\right) = -\frac{1}{\tau} a_{ego}\left(k\right) + \frac{1}{\tau} u(k) \tag{41}$$

where j_{ego} is the actual longitudinal jerk of the ego vehicle.

The state variable is defined as follows:

$$x(k) = \left[\Delta s\left(k\right), v_{ego}\left(k\right), v_{rel}\left(k\right), a_{ego}\left(k\right), j_{ego}\left(k\right)\right]^T \tag{42}$$

The controlled output vector is defined as follows:

$$y(k) = \left[\sigma\left(k\right), v_{rel}\left(k\right), a_{ego}\left(k\right), j_{ego}\left(k\right)\right]^T \tag{43}$$

Then from Eq. (37) - Eq. (43), state-space equations which represent longitudinal kinematics of an ACC-equipped vehicle and its preceding vehicle are presented:

$$x\left(k+1\right) = A_0 x\left(k\right) + B_0 u\left(k\right) + G_0 w(k) \tag{44}$$

$$y\left(k\right) = C_0 x\left(k\right) - Z_0 \tag{45}$$

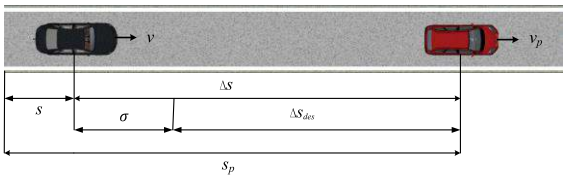

FIGURE 3. The schematic diagram of Vehicle-to-vehicle longitudinal kinematics model.

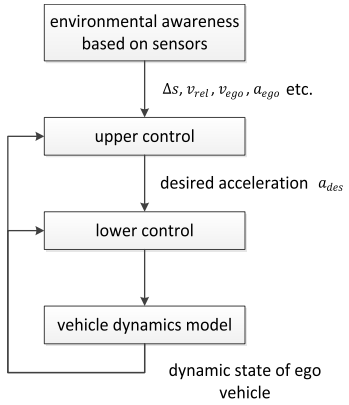

FIGURE 4. The hierarchical control structure of the ACC system.

where

$$A_0=\begin{bmatrix} 1 & 0 & T_s & -\frac{1}{2}T_s^2 & 0 \\ 0 & 1 & 0 & T_s & 0 \\ 0 & 0 & 1 & -T_s & 0 \\ 0 & 0 & 0 & 1-\frac{T_s}{\tau} & 0 \\ 0 & 0 & 0 & -\frac{1}{\tau} & 0 \end{bmatrix},\ B_0=\begin{bmatrix} 0 \\ 0 \\ 0 \\ \frac{T_s}{\tau} \\ \frac{1}{\tau} \end{bmatrix},\ G_0=\begin{bmatrix} \frac{1}{2}T_s^2 \\ 0 \\ T_s \\ 0 \\ 0 \end{bmatrix},$$

$$C_0=\begin{bmatrix} 1 & -t_h & 0 & 0 & 0 \\ 0 & 0 & 1 & 0 & 0 \\ 0 & 0 & 0 & 1 & 0 \\ 0 & 0 & 0 & 0 & 1 \end{bmatrix},\ Z_0=\begin{bmatrix} d_0 \\ 0 \\ 0 \\ 0 \end{bmatrix}.$$

B. MLD MODELING OF ACC UPPER CONTROL SYSTEM CONSIDERING SENSOR FAULTS

The ACC system typically use a hierarchical control structure [22], as shown in Fig.4.

It can be seen from Fig.4 that inputs of the ACC upper control system are motion information of the ego vehicle and surrounding vehicles acquired by each vehicle-borne sensor, and the output is the desired longitudinal acceleration which is the control input to be solved by the ACC upper control model. In order to realize the active fault tolerant ACC system, it is necessary to consider conditions of sensor faults when establishing the ACC upper control model.

The mixed logical dynamical (MLD) model is a kind of hybrid system which was first introduced by Bemporad *et al.* [23]. It can integrate the continuous state, discrete state, and constraints of the system into a unified framework, and then find a control sequence to satisfy the constraint and optimize the control objective function [24]. In this paper, sensor faults are taken as discrete events, and a MLD model of ACC upper control system is built which includes both fault-free dynamics and fault dynamics of the system.

When establishing the MLD model of ACC upper control system, a binary logic variable δ is introduced to describe the system's switching in conditions of no sensor fault and sensor faults:

$$\delta(k)=1 \leftrightarrow \delta 1_{same}(k)=1 \text{or} \delta 2_{same}(k)=1 \tag{46}$$

Then Eq. (44) is expressed as:

$$\begin{aligned} x(k+1) &= \{A_0x(k)+B_0u(k)+G_0w(k)\}(1-\delta(k)) \\ &\quad +\{A_1x(k)+B_1u(k)+G_1w(k)\}\delta(k) \end{aligned} \tag{47}$$

Sensor faults would cause the state variable $x(k)$ and the disturbance variable $w(k)$ to be discontinuous with the condition of no sensor fault. Therefore, when sensor faults occur, the dynamic state of the target vehicle is estimated according to the state estimation method in section II, i.e.:

$$\begin{cases} x(k)=\hat{x}(k) \\ w(k)=\hat{w}(k), \quad \delta=1, \end{cases} \tag{48}$$

Then Eq. (47) is simplified as:

$$\begin{aligned} x(k+1) &= A_0\left[x(k)(1-\delta)+\hat{x}(k)\delta\right] \\ &\quad +B_0u(k)+G_0\left[w(k)(1-\delta)+\hat{w}(k)\delta\right] \end{aligned} \tag{49}$$

$$y(k)=C_0\left[x(k)(1-\delta)+\hat{x}(k)\delta\right]-Z_0 \tag{50}$$

Introducing an auxiliary variable $z(k) = [z_1(k), z_2(k), z_3(k), z_4(k), z_5(k), z_6(k)]^T$:

$$\begin{cases} P_1z(k)=\begin{bmatrix} z_1(k) \\ z_2(k) \\ z_3(k) \\ z_4(k) \\ z_5(k) \end{bmatrix}=x(k)(1-\delta)+\hat{x}(k)\delta \\ P_2z(k)=[z_6(k)]=w(k)(1-\delta)+\hat{w}(k)\delta \end{cases} \tag{51}$$

where $P_1=\begin{bmatrix} 1&0&0&0&0&0 \\ 0&1&0&0&0&0 \\ 0&0&1&0&0&0 \\ 0&0&0&1&0&0 \\ 0&0&0&0&1&0 \end{bmatrix}$, $P_2=\begin{bmatrix} 0\\0\\0\\0\\0\\1 \end{bmatrix}^T$.

Then,

$$x(k+1)=A_0P_1z(k)+B_0u(k)+G_0P_2z(k) \tag{52}$$

$$y(k)=C_0P_1z(k)-Z_0 \tag{53}$$

Express Eq. (52) and Eq. (53) as standard forms of MLD model:

$$x(k+1)=Ax(k)+B_1u(k)+B_2\delta(k)+B_3z(k) \tag{54}$$

$$y(k)=Cx(k)+D_1u(k)+D_2\delta(k)+D_3z(k)+D_4 \tag{55}$$

where $A=0, B_1=B_0, B_2=0, B_3=A_0P_1+G_0P_2, C=0, D_1=0, D_2=0, D_3=C_0P_1, D_4=-Z_0$.

Convert the above propositional logic into following mixed integer inequalities:

1) Inequality constraints caused by introducing the auxiliary variable $z(k)$:

$$\begin{cases} (m_{12}-M_{11})\,\delta(k)+P_1z(k)\le x(k) \\ (m_{11}-M_{12})\,\delta(k)-P_1z(k)\le -x(k) \\ (m_{11}-M_{12})\,(1-\delta(k))+P_1z(k)\le \hat{x}(k) \\ (m_{12}-M_{11})\,(1-\delta(k))-P_1z(k)\le -\hat{x}(k) \end{cases} \tag{56}$$

$$\begin{cases} (m_{22}-M_{21})\,\delta(k)+P_2z(k)\le w(k) \\ (m_{21}-M_{22})\,\delta(k)-P_2z(k)\le -w(k) \\ (m_{21}-M_{22})\,(1-\delta(k))+P_2z(k)\le \hat{w}(k) \\ (m_{22}-M_{21})\,(1-\delta(k))-P_2z(k)\le -\hat{w}(k) \end{cases} \tag{57}$$

where $M_{11}=\max\hat{x}(k)=[\Delta\hat{s}(k),v_{max},\hat{v}_{rel}(k),a_{max},j_{max}]^T$, $m_{11}=\min\hat{x}(k)=[\Delta\hat{s}(k),v_{min},\hat{v}_{rel}(k),a_{min},j_{min}]^T$, $M_{12}=\max x(k)=\left[\Delta s_{max},v_{max},v_{rel\_max},a_{max},j_{max}\right]^T$, and $m_{12}=\min x(k)=\left[d_c,v_{min},v_{rel\_min},a_{min},j_{min}\right]^T$.

w is a_p, which is the longitudinal acceleration of the target vehicle. When the millimeter wave radar sensor is operating normally, $M_{22}=\max w(k)=a_{x\_max}$, and $m_{22}=\min w(k)=a_{x\_min}$. When false detection or missing detection of radar sensor occurs, the estimated value of the longitudinal relative acceleration of the target vehicle $\Delta\hat{a}_x(k)$ can be obtained by the method in section II.A, and then $\hat{w}(k)=\Delta\hat{a}_x(k)+a_{ego}(k)$. Then, we take $M_{21}=\max\hat{w}(k)=\hat{w}(k)$, and $m_{21}=\min\hat{w}(k)=\hat{w}(k)$.

2)value range constraints of the state variable $x(k)$ and the control input $u(k)$ of the ACC upper control model:

$$m_{12}\le x(k)\le M_{12} \tag{58}$$

$$u_{min}\le u(k)\le u_{max} \tag{59}$$

Convert the above inequality constraints into the standard constraint form of MLD model:

$$E_2\delta(k)+E_3z(k)\le E_1u(k)+E_4x(k)+E_5 \tag{60}$$

where

$$E_2=\begin{bmatrix} m_{12}-M_{11}\\ m_{11}-M_{12}\\ m_{22}-M_{21}\\ m_{21}-M_{22}\\ M_{12}-m_{11}\\ M_{11}-m_{12}\\ M_{22}-m_{21}\\ M_{21}-m_{21}\\ 0_{4\times1}\\ 0_{4\times1}\\ 0\\ 0 \end{bmatrix},\quad E_3=\begin{bmatrix} P_1\\ -P_1\\ P_2\\ -P_2\\ P_1\\ -P_1\\ P_2\\ -P_2\\ 0_{4\times6}\\ 0_{4\times6}\\ 0_{1\times6}\\ 0_{1\times6} \end{bmatrix},\quad E_1=\begin{bmatrix} 0_{5\times1}\\ 0_{5\times1}\\ 0\\ 0\\ 0_{5\times1}\\ 0_{5\times1}\\ 0\\ 0\\ 0_{4\times1}\\ 0_{4\times1}\\ 1\\ -1 \end{bmatrix},$$

$$E_4=\begin{bmatrix} I_{5\times5}\\ -I_{5\times5}\\ 0_{1\times5}\\ 0_{1\times5}\\ I_{5\times5}\\ -I_{5\times5}\\ 0_{1\times5}\\ 0_{1\times5}\\ 0_{1\times5}\\ 0_{1\times5}\\ 0_{1\times5}\\ 0_{1\times5} \end{bmatrix},\quad E_5=\begin{bmatrix} 0_{5\times1}\\ 0_{5\times1}\\ w(k)\\ -w(k)\\ M_{12}-m_{11}\\ M_{11}-m_{12}\\ \hat{w}(k)+M_{22}-m_{21}\\ -\hat{w}(k)+M_{21}-m_{22}\\ -m_{12}\\ M_{12}\\ -u_{min}\\ u_{max} \end{bmatrix}.$$

Eq. (54), Eq. (55) and Eq. (60) are the MLD model of ACC upper control system that contains conditions of sensor faults.

IV. ACTIVE FAULT TOLERANT CONTROL MODEL OF VEHICLE ACC SYSTEM BASED ON THE MPC FRAMEWORK

In section 3, sensor faults are taken as discrete events, and the MLD model of ACC upper control system is built which includes both fault-free dynamics and fault dynamics of the system. In section 4, based on a model predictive control (MPC) framework and the MLD model of ACC upper control system, an active fault tolerant control model of vehicle ACC system is established, so that the ACC-equipped vehicle can still drive safely and steadily when the millimeter-wave radar sensor fails.

MPC has three basic characteristics: model prediction, rolling optimization and feedback correction. Based on the standard MLD model of Eq. (54) and Eq. (55), and considering the feedback correction, the following prediction model can be recursively obtained:

$$\begin{aligned} &\hat{x}(k+p) \\ &=A^px(k)+\left[\sum_{i=p-m}^{p-1}A^iB_1u(k+p-1-i)\right. \\ &\quad\left.+\sum_{i=0}^{p-m-1}A^iB_1u(k+m-1)\right] \\ &\quad+\sum_{i=0}^{p-1}A^i\left[B_2\delta(k+p-1-i)\right. \\ &\quad\left.+B_3z(k+p-1-i)\right]+e_x(k) \end{aligned} \tag{61}$$

$$\begin{aligned} &\hat{y}(k+p) \\ &=CA^px(k)+\left[\sum_{i=p-m}^{p-1}CA^iB_1u(k+p-1-i)\right. \\ &\quad\left.+\sum_{i=0}^{p-m-1}CA^iB_1u(k+m-1)\right] \\ &\quad+\sum_{i=0}^{p-1}CA^i[B_2\delta(k+p-1-i)+B_3z(k+p-1-i) \\ &\quad+e_x(k+p-1-i)]+e_x(k)+D_1u(k+p) \\ &\quad+D_2\delta(k+p)+D_3z(k+p)+D_4 \end{aligned} \tag{62}$$

where p is the prediction horizon, m is the control horizon. When $p>m-1$, $u(k+p)=u(k+m-1)$. $e_x(k)$ is the error between measured system state value and predicted system state value in the k th period. $e_x(k)=x(k)-\hat{x}(k|k-1)$. The prediction model can be feedback corrected through $e_x(k)$.

In the $\boldsymbol{k}$ th period, the performance indicator for MPC is:

$$\min J = \sum_{i=0}^{m-1} \|u(k+i)\|^2_{R_u} + (1-\delta(k)) \sum_{i=0}^{m-1} \|\Delta u(k+i)\|^2_{R_{\Delta u}} + \sum_{j=1}^{p} \left\|y(k+j) - y_{ref}(k+j)\right\|^2_{Q_y} \quad (63)$$

where R_u, $R_{\Delta u}$, Q_y are weight coefficients, $\Delta u(k)$ is the change rate of $u(k)$: $\Delta u(k) = u(k) - u(k-1)$, $y_{ref}(k)$ is the reference trajectory of controlled output vector $y(k)$.

$$y_{ref}(k+i) = (1-\delta(k))\,\varphi^i y(k) + \delta(k)\, y_e \quad (64)$$

When there is no sensor failure, according to the reference [25], the smoother the change of parameters such as speed and acceleration, the lower the fuel consumption, and the better the fuel economy. Therefore, make y approach to the optimal value along the smooth reference trajectory to smooth the response curve and improve the fuel economy. When sensor faults occur, the safety of the ego vehicle is the primary consideration.

In Eq.(63), $\varphi = \begin{bmatrix} \rho_\sigma & 0 & 0 & 0 \\ 0 & \rho_v & 0 & 0 \\ 0 & 0 & \rho_a & 0 \\ 0 & 0 & 0 & \rho_j \end{bmatrix}$, $\rho_\sigma = e^{\frac{-T_s}{\alpha_\sigma}}$ $(0 < \rho_\sigma < 1)$, $\rho_v = e^{\frac{-T_s}{\alpha_v}}$ $(0 < \rho_v < 1)$, $\rho_a = e^{\frac{-T_s}{\alpha_a}}$ $(0 < \rho_a < 1)$, $\rho_j = e^{\frac{-T_s}{\alpha_j}}$ $(0 < \rho_j < 1)$ are coefficients of the reference trajectory corresponding to $\sigma(k)$, $v_{rel}(k)$, $a_{ego}(k)$, $j_{ego}(k)$. α_σ, α_v, α_a, α_j are time constants of the reference trajectory. $y_e(k) = [0, 0, 0, 0]^T$.

One of constraints is the constraint of the MLD model described above which contains conditions of sensor faults:

$$E_2\delta(k) + E_3 z(k) \le E_1 u(k) + E_4 x(k) + E_5 \quad (65)$$

Meanwhile, in order to limit the fluctuation of $u(k)$, $\Delta u(k)$ is constrained as follows:

$$\Delta u_{min} \le \Delta u(k) \le \Delta u_{max} \quad (66)$$

Under the framework of MPC, the ACC upper control system is transformed into the online quadratic optimization problem with constraints, as shown by equations (63), (65), and (66). In the $\boldsymbol{k}$ th period, we solve the above optimization problem by the quadratic programming solver in the Matlab Optimization Toolbox, and obtain optimal control sequences of the future system: $u(k)$, $u(k+1)$, $\ldots$, $u(k+m-1)$, then apply the first control variable $u(k)$ to the system. Repeat the above operations in the $\boldsymbol{k+1}$ th period to achieve rolling optimization.

Note here that active fault tolerant control model is aimed at the ACC upper control. The MPC framework is used to perform rolling real-time optimal control of the ACC upper system. As hierarchical control is adopted, after the desired longitudinal acceleration a_{des} and the desired velocity v_{des} of the ego vehicle are obtained by the upper control, increment PID control algorithm is adopted in lower control to calculate the desired throttle opening θ_{des} and the desired brake pressure P_{b_des}. θ_{des} and P_{b_des} are used as inputs to the vehicle dynamics model in order to control the actual acceleration following the desired acceleration a_{des}.

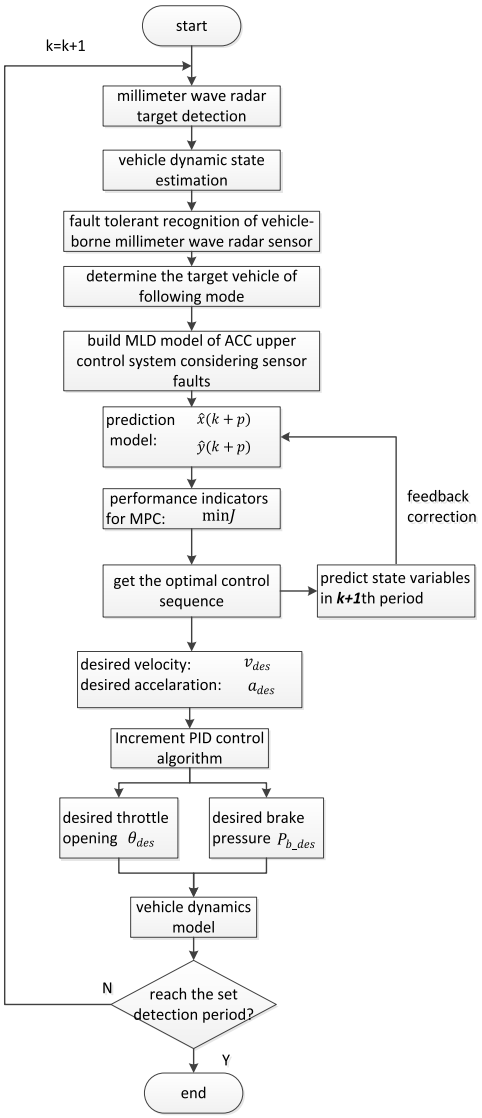

FIGURE 5. The structure diagram of this active fault tolerant control model of vehicle ACC system based on the MPC framework.

The essence of the above active fault tolerant control model of ACC system is: introduce sensor faults into the model of ACC upper control system. When radar faults occur, the system is switched to the fault state on the model side, and the model and constraints are changed to reconstruct the model predictive controller. The new performance indicator is optimized, and the control input value in the fault state is solved to achieve the purpose of fault tolerant control. The structure diagram of this active fault tolerant control model of ACC system based on the MPC framework shown in Fig.5.

V. SIMULATION AND ANALYSIS

A. SIMULATION PLATFORM AND PARAMETERS

In this paper, PreScan is used to test the active fault tolerant control model of ACC system based on the MPC framework.

FIGURE 6. The simulation scene of the ACC system.

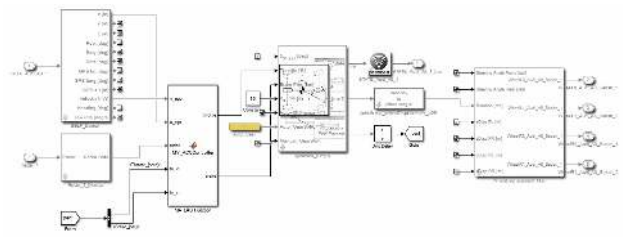

FIGURE 7. Structure diagram of the Co-simulation interface.

PreScan is a kind of software applied in advanced auxiliary driving system and intelligent vehicle system studied by the Netherlands national academy of applied sciences [26]. Due to simple operation and good real-time performance, it has been widely used in researches and tests of auxiliary driving and driverless cars.

The modeling process of PreScan is divided into four parts: the construction of simulation scene, the establishment of sensor model, the addition of control system and the running of simulation experiment. For the ACC system to be simulated, this paper built a multi-lane complex driving scenario in the GUI of PreScan, including 8-lane dual carriageway with traffic signs, as shown in Fig.6. The ego vehicle is equipped with millimeter wave radar to obtain the relative distance and relative velocity between the ego vehicle and surrounding vehicles. Observation noises are added to the radar sensor. The control system is added to the Co-simulation interface of PreScan and Simulink, as shown in Fig.7.

Simulation parameters are shown in Table 1.

According to the road width standard of motorway in China, the lane width in simulation is 3.5 meters.

When the Sage-Husa adaptive Kalman filter algorithm is used to estimate states of the target vehicle, initial conditions of the filtering are selected as follows: $\hat{Q}_0 = 0.85$, $R = \begin{bmatrix} R_0 & 0 \\ 0 & R_1 \end{bmatrix} = \begin{bmatrix} 0.01 & 0 \\ 0 & 0.001 \end{bmatrix}$, $P_0 = I$, $b = 0.985$, $\xi = 1.15$, and $\hat{X}_0 = [57.47, -7, 0, 0]^T$.

According to the structure diagram and simulation parameters, the proposed active fault tolerant control algorithm of vehicle ACC system was tested in the simulation traffic environment. Test results are as follows.

B. SIMULATION AND ANALYSIS

Through multiple simulation experiments and analyses, we found that in following extreme cases, even a short-term false detection and missing detection of the millimeter wave radar sensor would have a serious impact on vehicles. The definition of extreme cases is as follows:

If the velocity of the target vehicle decreases, the relative distance between two vehicles will decrease. When no sensor fails, under the control of ACC system, the velocity will be adjusted to maintain the desired relative distance. However, if sensor fails at this time, for example, the relative distance measured by the sensor is much larger than the actual relative distance, then ACC system will decide to accelerate. Then the actual relative distance will become too small, and even a rear-end collision will occur. In this paper, we show simulation results in these extreme cases.

In the simulation, we select two periods in which the target vehicle slowed down, and add sensor faults respectively. The false detection of radar sensor is added from 6.5s to 8.5s, which makes the relative distance and relative velocity measured by the millimeter wave radar sensor change radically. The missing detection of radar sensor is added from 28s to 30s, which makes the sensor's measurement value null. The simulation results are shown in Fig. 8-Fig.11.

Fig.8 is the velocity response curve of the vehicle equipped with the conventional ACC system in the condition of false detection. Fig.9 is the velocity response curve of the vehicle equipped with the conventional ACC system in the condition of missing detection. Fig.10 is the velocity response curve of the vehicle equipped with the fault tolerant ACC system proposed in this work in the conditions of false detection and missing detection, and the sign value of sensor faults. Fig.11 is the relative distance response curve in the conditions of false detection and missing detection. In those figures, V_A is the velocity of the ego vehicle, V_B − sensor is the velocity of the target vehicle detected by the millimeter wave radar sensor, V_B − actual is the actual velocity of the target vehicle,

TABLE 1. Simulation parameters.

Symbol	Quantity	Value
T	radar sampling frequency	10Hz
T_s	sampling period of ACC upper system	0.1s
τ	time constant of the lower control	0.5s
t_{TTC}	time-to-collision	2.5
Y_{same}	threshold value of the same lane	2m
Y_{adj}	threshold value of adjacent lanes	4m
p	prediction horizon	16
m	control horizon	5
d_c	minimum safe distance between two vehicles	5m
Δs_{max}	minimum distance limit between two vehicles	60
v_{min}	Minimum velocity limit of the ego vehicle	0
v_{max}	Maximum velocity limit of the ego vehicle	30m/s
a_{min}	Minimum acceleration limit of the ego vehicle	-8m/s^2
a_{max}	Maximum acceleration limit of the ego vehicle	2.5m/s^2
j_{min}	Minimum jerk limit of the ego vehicle	-3 m/s^2
j_{max}	Maximum jerk limit of the ego vehicle	3 m/s^2
v_{rel_min}	Minimum v_{rel} limit of the ego vehicle	-10m/s
v_{rel_max}	Maximum v_{rel} limit of the ego vehicle	10m/s

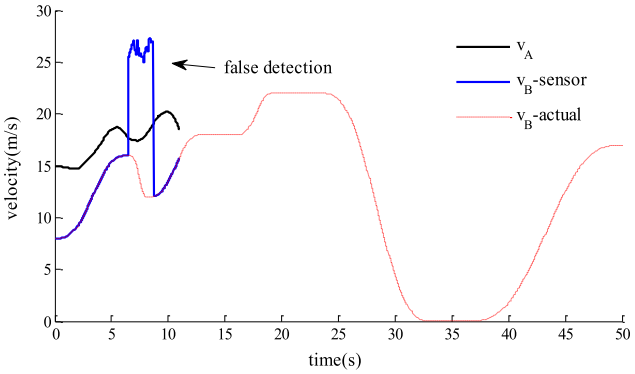

FIGURE 8. The velocity response curve of the vehicle equipped with the conventional ACC system in the condition of false detection.

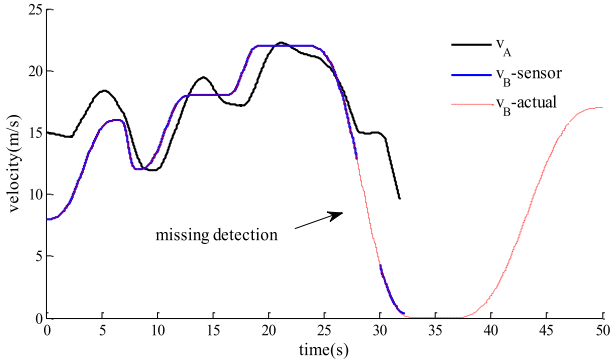

FIGURE 9. The velocity response curve of the vehicle equipped with the conventional ACC system in the condition of missing detection.

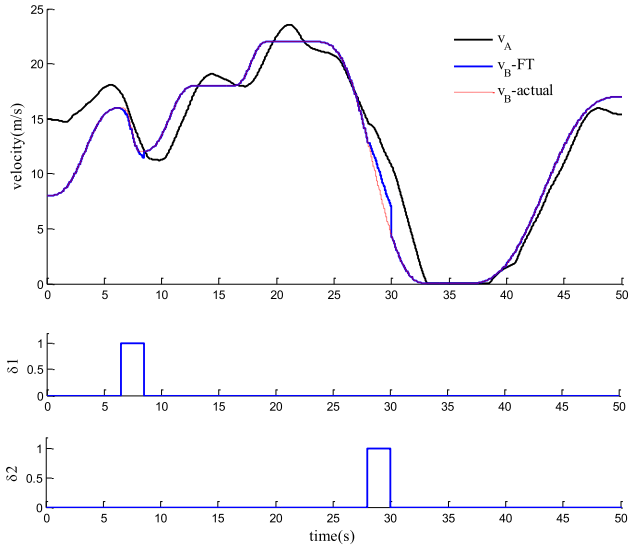

FIGURE 10. The velocity response curve of the vehicle equipped with the active fault tolerant ACC system in the conditions of false detection and missing detection, and the sign value of sensor faults.

and $V_B-\mathrm{FT}$ is the velocity of the target vehicle calculated by fault tolerant control method.

It can be seen from Fig.8 and Fig.11 that when false detection of radar sensor occurs (6.5s to 8.5s), the relative

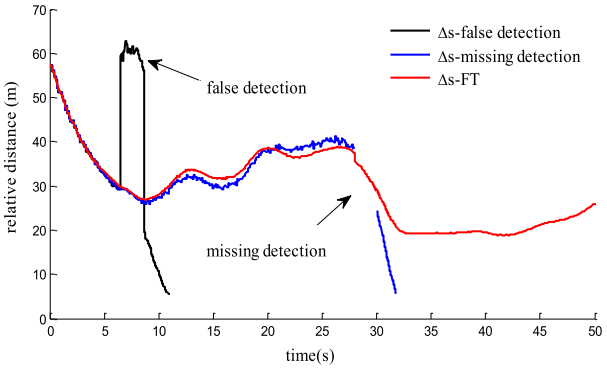

FIGURE 11. The relative distance response curve in the conditions of false detection and missing detection.

distance (black solid line in Fig.11) and the velocity of the target vehicle (blue solid line in Fig.8) are detected as abrupt changes. The conventional ACC system will consider it as a new target vehicle, and control ego vehicle to follow this fake target vehicle. When the radar sensor returns to normal, the actual relative distance and the velocity of the target vehicle are detected as abrupt changes again. Because during the period of false detection, the true target vehicle is decelerating, while ego vehicle is accelerating, the actual relative distance between the two vehicle drops rapidly. Although the conventional ACC system decides to decelerate when the radar sensor returns to normal, the relative distance still drops to the minimum safe distance d_c, which causes the conventional ACC system to fail to solve the control sequence that satisfies the constraints. That is to say, if ego vehicle continues drive, a real-end collision will occur.

It can be seen from Fig.9 and Fig.11 that when missing detection of radar sensor occurs (28s to 30s), the relative distance (blue solid line in Fig.11) and the velocity of the target vehicle (blue solid line in Fig.9) cannot be detected. The conventional ACC system will consider that there is no target vehicle in front, and switches to cruising mode, then controls the ego vehicle to drive at the set velocity 15m/s. When the radar sensor returns to normal, the actual relative distance and the velocity of the target vehicle are detected. During the period of missing detection, the actual target vehicle is decelerating, so the actual relative distance between the two vehicle decreases. Although the conventional ACC system decides to decelerate when the radar sensor returns to normal, the velocity of ego vehicle is still large. When the velocity of the target vehicle reduced to 0, the relative distance drops to the minimum safe distance d_c, which will also cause the conventional ACC system to fail to solve the control sequence that meets the constraints and lead to a real-end collision will occur.

For the same false detection and missing detection, the active fault tolerant control algorithm of ACC system proposed in this paper is used for simulation. It can be seen from Fig.10 and Fig.11 that when the false detection (6.5s to 8.5s) and missing detection (28s to 30s) of radar sensor occurs, the active fault tolerant ACC system recognizes

the false detection and missing detection respectively, and sets the sign value of sensor faults to 1. From the velocity curve of the target vehicle processed by active fault tolerant control algorithm (blue solid line in Fig.10) and the relative distance processed by active fault tolerant control algorithm (solid red line in Fig.11), it can be seen that the velocity after fault tolerance is basically the same as the actual velocity (red dotted line in Fig.10), and the relative distance is also always within a relatively stable range. That is to say, faults of the millimeter wave radar sensor don't cause any danger after using the active fault tolerant ACC algorithm.

VI. CONCLUSION

In this paper, sensor faults are taken as discrete events, and the MLD model of ACC upper control system is built which includes both fault-free dynamics and fault dynamics of the system. Based on the MPC framework, the active fault tolerant control model of ACC system is established. Combined with the PreScan vehicle simulation platform, the application of the proposed active fault tolerant control algorithm of ACC system is simulated and verified.

The simulation results show that the vehicle equipped with the active fault tolerant ACC system still drive safely and smoothly without being affected by radar sensor failures, while the vehicle equipped with the conventional ACC system is affected in these cases. Therefore, the active fault tolerant control model of ACC system proposed in this paper is of great significance to ensure the safe driving of intelligent vehicles.

It should be noted that since our work is a series of experiments, the simulation verification of the algorithm is currently carried out. Tests in the PreScan simulation platform can be done in real time. In the subsequent work, we will verify the proposed active fault tolerant control algorithm and its real-time performance on the actual vehicle. Of course, the model in this paper is not only used for ACC, but can also be used for other advanced driver assistance system technologies, such as collision avoidance system and lane change assist system.

REFERENCES

[1] G. Q. Wu, L. X. Zhang, and Z. Y. Liu, "Research status and development trend of vehicle adaptive cruise control systems," *J. Tongji Univ. (Natural Sci.)*, vol. 45, no. 4, pp. 544–553, Apr. 2017.

[2] N. Lydie and S. Mammar, "Experimental vehicle longitudinal control using a second order sliding mode technique," *Control Eng. Pract.*, vol. 15, no. 8, pp. 943–954, Aug. 2007.

[3] L.-H. Luo, H. Liu, P. Li, and H. Wang, "Model predictive control for adaptive cruise control with multi-objectives: Comfort, fuel-economy, safety and car-following," *J. Zhejiang Univ. Sci. A, Appl. Phys. Eng.*, vol. 11, no. 3, pp. 191–201, Mar. 2010.

[4] S. Li, K. Li, R. Rajamani, and J. Wang, "Model predictive multi-objective vehicular adaptive cruise control," *IEEE Trans. Control Syst. Technol.*, vol. 19, no. 3, pp. 556–566, May 2011.

[5] R. Dang, J. Wang, S. E. Li, and K. Li, "Coordinated adaptive cruise control system with lane-change assistance," *IEEE Trans. Intell. Transp. Syst.*, vol. 16, no. 5, pp. 2373–2383, Oct. 2015.

[6] R. Schmied, H. Waschl, and L. Del Re, "Comfort oriented robust adaptive cruise control in multi-lane traffic conditions," *IFAC-PapersOnLine*, vol. 49, no. 11, pp. 196–201, 2016.

[7] J. Hasch, E. Topak, R. Schnabel, T. Zwick, R. Weigel, and C. Waldschmidt, "Millimeter-wave technology for automotive radar sensors in the 77 GHz frequency band," *IEEE Trans. Microw. Theory Techn.*, vol. 60, no. 3, pp. 845–860, Mar. 2012.

[8] Z. H. Gao, J. Wang, and J. Tong, "Target motion state estimation for vehicle-borne millimeter-wave radar," *J. Jilin Univ. (Eng. Technol. Ed.)*, vol. 44, no. 6, pp. 1537–1544, Nov. 2014.

[9] H. Guo, D. Cao, H. Chen, C. Lv, H. Wang, and S. Yang, "Vehicle dynamic state estimation: State of the art schemes and perspectives," *IEEE/CAA J. Autom. Sinica*, vol. 5, no. 2, pp. 418–431, Mar. 2018.

[10] C. Wu, Y. Lin, and A. Eskandarian, "Cooperative adaptive cruise control with adaptive Kalman filter subject to temporary communication loss," *IEEE Access*, vol. 7, pp. 93558–93568, 2019.

[11] G. Guo and W. Yue, "Sampled-data cooperative adaptive cruise control of vehicles with sensor failures," *IEEE Trans. Intell. Transp. Syst.*, vol. 15, no. 6, pp. 2404–2418, Dec. 2014.

[12] E. V. Nunen, J. Ploeg, and A. M. Medina, "Fault tolerancy in cooperative adaptive cruise control," presented at the 16th Int. IEEE Conf. Intell. Transp. Syst. (ITSC), 2013. [Online]. Available: https://ieeexplore.ieee.org/document/6728393/

[13] M. R. Boukhari, A. Chaibet, M. Boukhnifer, and S. Glaser, "Two longitudinal fault tolerant control architectures for an autonomous vehicle," *Math. Comput. Simul.*, vol. 156, pp. 236–253, Feb. 2019.

[14] H. Fang, N. Tian, Y. Wang, M. Zhou, and M. A. Haile, "Nonlinear Bayesian estimation: From Kalman filtering to a broader horizon," *IEEE/CAA J. Autom. Sinica*, vol. 5, no. 2, pp. 401–417, Mar. 2018.

[15] T. Y. Xiao, Y. Y. Zhang, and J. D. Chen, *Introduction to System Simulation*. Beijing, China: TUP, 2000, pp. 56–72.

[16] C. Miyajima, H. Ukai, A. Naito, H. Amata, N. Kitaoka, and K. Takeda, "Driver risk evaluation based on acceleration, deceleration, and steering behavior," presented at the IEEE Int. Conf. Acoust., Speech, Signal Process. (ICASSP), 2011. [Online]. Available: https://ieeexplore.ieee.org/document/5946860

[17] X. Y. Lu and J. Wang, "Multiple-vehicle longitudinal collision avoidance and impact mitigation by active brake control," presented at the IEEE Intell. Vehicles Symp., 2012. [Online]. Available: https://ieeexplore.ieee.org/document/6232246

[18] Z. W. Feng, X. H. Ma, X. C. Zhu, and Z. X. Ma, "Analysis of driver brake behavior under critical cut-in scenarios," presented at the IEEE Intell. Vehicles Symp. (IV), 2018. [Online]. Available: https://ieeexplore.ieee.org/document/8500438

[19] Y. H. Chiang and J. C. Juang, "Longitudinal vehicle control with the spacing policy in consideration of brake input limits," presented at the IEEE Int. Conf. Syst., Man, Cybern., 2007. [Online]. Available: https://ieeexplore.ieee.org/document/4413810

[20] V. Rajaram and S. C. Subramanian, "Heavy vehicle collision avoidance control in heterogeneous traffic using varying time headway," *Mechatronics*, vol. 50, pp. 328–340, Apr. 2018.

[21] J.-J. Martinez and C. Canudas-de-Wit, "A safe longitudinal control for adaptive cruise control and stop-and-go scenarios," *IEEE Trans. Control Syst. Technol.*, vol. 15, no. 2, pp. 246–258, Mar. 2007.

[22] G. Feng, "Multi-model based hierarchical switching control for vehicle longitudinal motion," Ph.D. dissertation, Dept. Autom. Eng., Tsinghua Univ., Beijing, China, 2006.

[23] A. Bemporad and M. Morari, "Control of systems integrating logic, dynamics, and constraints," *Automatica*, vol. 35, no. 3, pp. 407–427, Mar. 1999.

[24] X. Sun, Y. Cai, S. Wang, X. Xu, and L. Chen, "Optimal control of intelligent vehicle longitudinal dynamics via hybrid model predictive control," *Robot. Auto. Syst.*, vol. 112, pp. 190–200, Feb. 2019.

[25] S. E. Li, Z. Jia, K. Li, and B. Cheng, "Fast online computation of a model predictive controller and its application to fuel economy–oriented adaptive cruise control," *IEEE Trans. Intell. Transp. Syst.*, vol. 16, no. 3, pp. 1199–1209, Jun. 2015.

[26] G. Xiong, H. Li, Z. Ding, J. Gong, and H. Chen, "Subjective evaluation of vehicle active safety using PreScan and Simulink: Lane departure warning system as an example," presented at the IEEE Int. Conf. Veh. Electron. Saf. (ICVES), 2017. [Online]. Available: https://ieeexplore.ieee.org/document/7991927

HUA ZHANG (Fellow, IEEE) was born in Xi'an, Shanxi, China, in 1992. She received the B.Tech. and M.S. degrees from the College of Control and Computer Engineering, North China Electric Power University, Beijing, China, in 2014 and 2017, respectively. She is currently pursuing the Ph.D. degree with the College of Control Science and Engineering, Zhejiang University.

Her research interest includes fault-tolerant control of intelligent vehicle and driver-assistance systems.

JUN LIANG was born in May 1963. He received the B.Tech. degree from the Department of Automation, Tsinghua University, in 1984, and the M.S. and Ph.D. degrees from the College of Control Science and Engineering, Zhejiang University, Hangzhou, China, in 1988 and 1993, respectively.

He has been a Professor and the Ph.D. Tutor with the College of Control Science and Engineering, Zhejiang University.

ZHIYUAN ZHANG was born in Taiyuan, Shanxi, China, in 1995. He received the B.Tech. degree from the College of Electronic Information, Sichuan University, Chengdu, China, in 2017. He is currently pursuing the Ph.D. degree with the College of Control Science and Engineering, Zhejiang University.